Design of High Entropy Superalloy FeNiCrAlCu using Computational Thermodynamic and Machine Learning: Effect of Alloying Compositions and Temperatures on the Stacking Fault Energy

Tria Laksana Achmad[1*] and *Farrel* Faiz Baskara[1]

[1]Department of Metallurgical Engineering, Institut Teknologi Bandung, 40132 Bandung, Indonesia

Abstract. High entropy superalloys (HESA) have great potential to replace superalloys with promising properties extensively developed to improve performance, resource sustainability, and cost efficiency in high-temperature applications. This study focuses on Fe-based HESA and their stacking fault energy (SFE), a critical parameter influencing deformation mechanism and creep resistance. This development is economically cheaper since it utilizes Fe rather than Ni as the alloy base, which has been widely developed. We propose a novel approach for predicting SFE using big data analysis leveraging machine learning and computational thermodynamics. The calculated SFE as a function of compositions and temperature becomes the database for the machine learning model. We employ a deep learning neural network model to achieve an impressive 0.008 Root Mean Squared Error (RMSE) predicting SFE values and classes. The composition of the high entropy superalloy is designed to lower the SFE, which promotes the formation of stacking faults and twin boundaries, resulting in high strength and creep resistance at high temperatures. Our research establishes an optimal design guide for achieving desired SFE: Ni (9-15 at%), Cr (15-36 at%), Al (5-22.75 at%), Cu (9-22.75 at%), and Fe (22.75-40 at%). Fe can be increased until 40 at.% with 15 at.% Ni, or Ni can be reduced until 9 at.% with a lower Fe of 22.75 at.%.

1 Background

Superalloys are nickel, iron-nickel, and cobalt-based alloys used as high-temperature material components due to their excellent heat resistance properties[1]. Nickel-based superalloys are often used in the energy, oil, gas, and aviation sectors as critical components of turbine engines[2-3]. These superalloys rely on coherent dispersion of $Ni_3(Al,Ti)$-based $L1_2$ γ' precipitates in an FCC-γ matrix to produce high strength at high temperatures. To operate at higher temperatures, adding refractory elements such as Mo, W, Ta, Re, or Ru can form a superalloy capable of operating well above its melting temperature and producing high creep resistance at high temperatures[4]. However, as refractory elements are expensive metals, their addition has the potential to limit the application range of such alloys.

To obtain better cost-performance alloys, high entropy alloys (HEA) allow the option of utilizing a more expansive compositional space[5]. HEA are a new class of materials with diverse multi-principal elements and interesting property-structure relationships[6]. HEA is defined to have at least 5 main elements ranging from 5 - 35 at.%. High entropy is a term coined based on the idea that a single phase of a solid solution can be stabilized through a high entropy configuration or $|\Delta S_{mix}|$ value > 1.5R[7], which is associated with the random mixing of several elements with similar atomic fractions[8].

In its development, nickel-rich HEA became a breakthrough for improving the thermal stability of the matrix γ and precipitating γ' phase microstructures that improved the alloy's strength at high temperatures. Nickel-rich HEAs with γ and γ' matrix microstructures resemble the microstructure of superalloys, so the material class is named High Entropy Superalloys (HESA)[5]. HESA has the advantage of having low density and manufacturing prices compared to superalloys. In addition, HESA offers excellent high-temperature mechanical properties, such as high mechanical strength, corrosion resistance, oxidation resistance, and creep resistance [4]. The development of HESA involves superalloy elements such as Fe, Ni, Al, Ti, Cr, and Co, for example, FeNiCoCrAl[9] and $Fe_{45}Ni_{25}Cr_{-25}Mo_5$-based alloys[10]. Given the relatively expensive elements Co and Mo, it is necessary to develop variations involving cheaper elements such as Cu. Cu has a relatively low price in alloy manufacturing[11], and adding Cu can also increase the toughness of the alloy[12]. Huang et al. show that adding Cu in the high entropy alloy $AlCrFeNiTiCu_x$ increased the ductility but decreased the hardness and wear resistance because it hindered the FCC phase formation[13]. FeNiCrAlCu is a new alloy development

* Corresponding author: tria_laksana@itb.ac.id

classified as iron-based HESA. This alloy has not yet been extensively analyzed for its properties and strength at elevated temperatures.

One of the critical properties in materials that are very important to evaluate, especially in high-temperature materials, is creep resistance[14]. Creep resistance refers to the ability of a material to withstand long-term loads or stresses at high temperatures[15]. Stacking Fault Energy (SFE) is one of the values that can describe the creep behavior of a material. SFE defines as the energy required to form a stacking fault per unit area in the material's atomic structure. SFE can describe the dominant deformation behavior of slip mode, twinning deformation, and martensitic or FCC-HCP transformation of a material[16]. A low SFE value means the distance between two partial dislocations is wide, preventing complete dislocation and inhibiting cross slip. Such events can restrain the creep rate.

The approach to measuring the SFE is usually done experimentally through the Transmission Electron Microscopy (TEM) method. The TEM method is theoretically reliable in SFE measurement, but there are several limitations, such as that measurements are challenging to perform and require significant time and cost[17]. Computational methods have emerged as an alternative to calculate the SFE. Computational methods are used to design a metal alloy using computer capabilities to simulate, calculate, and analyze an alloy composition to achieve the desired microstructure and properties[18]. One example of a computational method is the first-principle density functional theory (DFT) method based on quantum mechanical theory. However, this method takes a relatively long time to simulate and optimize. Therefore, machine learning methods are a new alternative to predicting the SFE of an alloy. The machine learning method requires extensive data to predict the SFE. Thus, the computational thermodynamics method is used to simulate the SFE value, and the results become the database of the machine learning model. This study simulated the effect of Fe-based HESA FeNiCrAlCu compositions and temperatures on the SFE. The simulation was carried out using computational methods based on thermodynamic calculations and machine learning.

2 Computational Procedure

A series of simulations were conducted using thermodynamic calculation and machine learning methods to study the effect of composition and temperature variations on the SFE of high entropy superalloy FeNiCrAlCu. The simulation flowchart is briefly shown in Fig. 1. Thermodynamic calculations using MATLAB software and machine learning modeling simulations using Jupyter Notebook software with the help of TensorFlow. The results of the SFE calculation from computational thermodynamics are then used as a database to interpret the relationships and patterns that occur and then become input for machine learning models that can learn patterns from the data and predict the value and classification of the SFE.

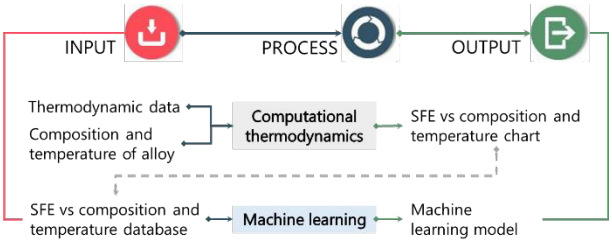

Fig. 1. Flowchart of computational thermodynamic and machine learning simulation in this study.

2.1 Computational Thermodynamic Method

Stacking fault energy modeling considers the phenomenon of phase transformation change from γ-FCC to ε-hcp of the thin plate ($\Delta G^{\gamma\to\varepsilon}$) by involving the interface energy ($\sigma^{\gamma/\varepsilon}$) as illustrated in Fig. 2. Then the SFE can be calculated:

$$\gamma_{sf} = 2\frac{4}{\sqrt{3}}\frac{1}{a^2 N}\Delta G^{\gamma\to\varepsilon} + 2\sigma^{\gamma/\varepsilon} \quad (1)$$

where γ_{sf} is the SFE value (mJ/m^2), the initial equation $\frac{4}{\sqrt{3}}\frac{1}{a^2 N}$ is the value of atomic density (ρ), which a is the lattice parameter, and N is Avogadro's constant. The value of the lattice parameter is a constant value of 3.58 Å, assuming there is no dependence between the lattice parameter and composition and temperature. This value is not too much different from the experimental lattice parameter using XRD of $AlCrCuFeNi_2$ (3.618 Å)[19]. $\Delta G^{\gamma\to\varepsilon}$ is the difference in Gibbs free energy at the FCC to hcp phase transformation, $\sigma^{\gamma/\varepsilon}$ is the interface energy per unit area of the phase boundary.

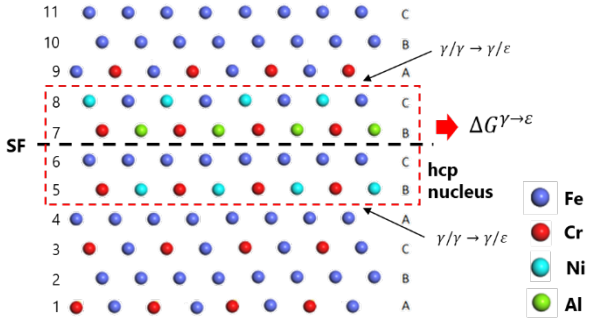

Fig. 2. Illustration of the stacking fault (SF) in an FCC crystal of HESA FeCrNiAlCu by computational dynamics.

In a multi-component alloy, the equation is extended to include the change value of the Gibbs energy of each element i ($\Delta G_i^{\gamma\to\varepsilon}$), the excess energy between elements i and j ($\Delta\Omega_{ij}^{\gamma\to\varepsilon}$) as well as the magnetic contribution to the Gibbs free energy ($\Delta G_{mg}^{\gamma\to\varepsilon}$), which is then the Gibbs free energy equation is written as:

$$\Delta G^{\gamma\to\varepsilon} = \sum_i X_i \Delta G_i^{\gamma\to\varepsilon} + \sum_{ij} X_i X_j \Delta\Omega_{ij}^{\gamma\to\varepsilon} + \Delta G_{mg}^{\gamma\to\varepsilon} \quad (2)$$

with X_i being the mole fraction of the corresponding element of each alloy. Full descriptions of the SFE calculations and the thermodynamic data used in this

calculation were presented in our previous study in Reference[17].

2.2 Machine Learning Method

The results of all thermodynamic calculations become the database of machine learning modeling. The database has 2340 data with the feature or input: alloy composition (in atomic percent) and temperature, while the target or output is the SFE. This modeling uses Jupyter Notebook software with the help of TensorFlow, an end-to-end open-source platform for machine learning. The flowchart of the modeling process is presented in Fig. 3.

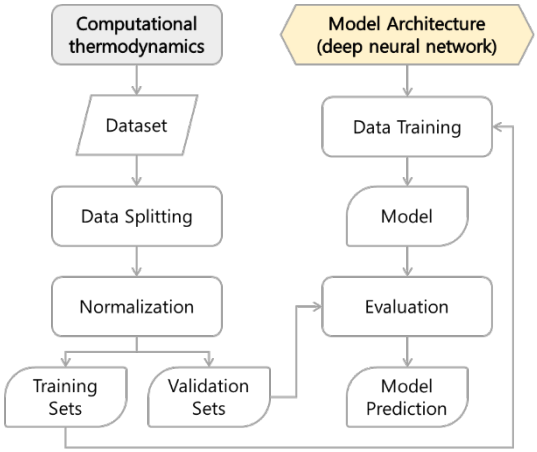

Fig. 3. Flowchart of machine learning processes in this study.

The modeling begins by entering the results of thermodynamic calculations as input, and then data preparation is carried out to retrieve the required features and targets. The data is then divided into training and validation data with a ratio of 80:20. Training data is data used to train a model to understand the patterns and correlations between features and targets in the database. Meanwhile, validation data is data that has never been seen by machine learning models before and is used to assess the accuracy of the predictions. After that, the model is evaluated by comparing the prediction results by machine learning with the actual results to choose the model with the best performance. The model is built using deep neural network architecture, trained in 10 epchs using adam optimizer and mean squared error loss function. After training, the model is evaluated using Root Mean Squared Error (RMSE) metrics. If the RMSE is good, then the model can be used for prediction.

3 Results and Discussion

3.1 Effect of Temperature on the SFE of HESA FeCrNiAlCu

The SFE of HESA FeCrNiAlCu increases with increasing temperature, as shown in Fig. 4. $\Delta G^{\gamma\to\varepsilon}$ is a function of temperature, then the increase or decrease of the SFE will depend on the temperature. Based on the Gibbs energy equation, which is $\Delta G = \Delta H - T\Delta S$, if the Gibbs energy function has a positive entropy, then increasing temperature will increase $\Delta G_{chemical}$, therefore increasing the SFE. Conversely, if the entropy is negative, an increase in temperature will decrease the SFE. Gholizadeh also found similar results for iron-based alloys Fe-Cr-Ni system, which showed a rise in SFE with increasing temperature[20]. The effect of temperature on SFE is mainly influenced by lattice expansion and the driving force for hcp to FCC phase transformation. In addition, research conducted by Zhang et al. through experiments using XRD showed that the decrease in the SFE of HEA CrCoFeMnNi alloy is due to the stabilization of the hcp phase at low temperatures, or in other words, the FCC phase is more stable with increasing temperature so that the SFE increases[21-22].

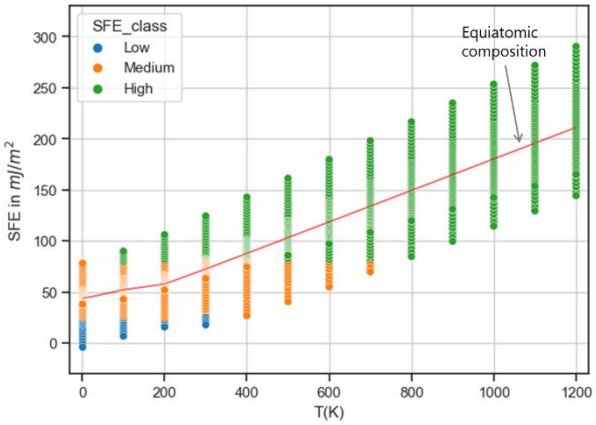

Fig. 4. Calculated SFE of HESA FeCrNiAlCu as a function of temperatures from thermodynamics calculation.

3.2 Effect of Alloying Compositions on the SFE of HESA FeCrNiAlCu

3.2.1 Effects of Ni concentrations on SFE

Fig. 5 shows that the SFE increases with the increase of Ni concentrations. For example, at a temperature of 300 K (Fig. 5(b)), the SFE increases from 56.35 mJ/m^2 to 100.52 mJ/m^2. The effect of temperature is also shown in Fig. 5(a) as the distribution vertically upwards at one composition point on the graph. The SFE will rise constantly as the temperature increases. A branching line from the equiatomic compositions in Fig. 5(b) shows the effect of other elements as the Ni concentration increases. The decrease in each element has a different impact on the SFE. Such as a decrease in Fe, Cu, and Cr increases the SFE, while a decrease in Al can reduce the SFE.

The effect of Ni concentrations on the SFE in this study is similar to the research conducted by Wang et al.[23]. They showed that the SFE rises simultaneously with increased Ni content through tensile testing of Cu-Ni alloys with a range of Ni from 5-20%. In addition, Zhao et al. showed similar results regarding the phase transformation in $CoCrNi_x$ medium entropy alloy[24]. The study analyzed that the intensity of the hcp phase

decreases as the Ni content increases, and according to thermodynamic calculations by Olson and Cohen, the SFE will increase.

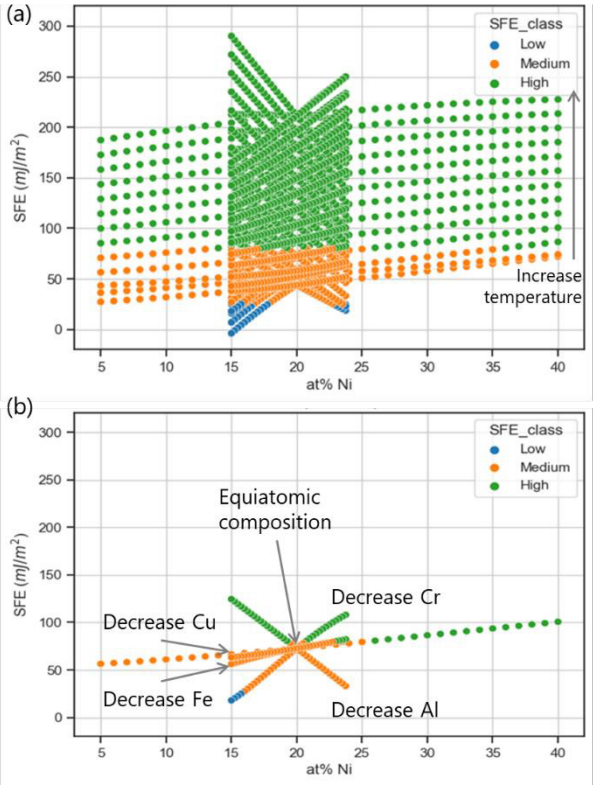

Fig. 5. Effect of Ni concentrations on the calculated SFE (a) at different temperatures from 1 to 1200 K and (b) at 300 K.

3.2.2 Effects of Cr concentrations on SFE

In contrast with the effect of Ni, increasing Cr concentrations will decrease the SFE, as shown in Fig. 6. Fig. 6(b) shows that at a temperature of 300 K, the SFE decreases from 107.89 mJ/m^2 to 17.97 mJ/m^2. The effect of temperature is also shown in Fig. 5(a), in which the SFE will rise as the temperature increases. Fig. 6(b) also shows the effect of other elements as the Cr concentration increases, in which a decrease in Fe and Cu increases the SFE, while a reduction of Al and Ni can reduce the SFE.

Similar results were also obtained by A. Dumay et al. in the paper on the effect of element addition on the SFE of Fe-Mn-C austenitic steel[25]. In Fe-22Mn0.6C steel, the addition of Cr element decreases the SFE. The tendency of Cr to reduce the SFE is also shown in the simulation conducted by Yan et al. with the Density Functional Theory (DFT) method on $CoCr_xNi$, which shows an increase in the intensity of the hcp phase along with an increase of Cr[26]. In this study, the increase in Cr content is related to the deformation of thin twinning, and the first principle DFT calculation indicates a decrease in SFE which may contribute to the appearance of nano-twins. In summary, the role of Cr in plastic deformation is to increase nano-twins and slip bands that occur during tensile processing. The effect of Twinning Induced Plasticity (TWIP) is the reason for the good ductility of the alloy.

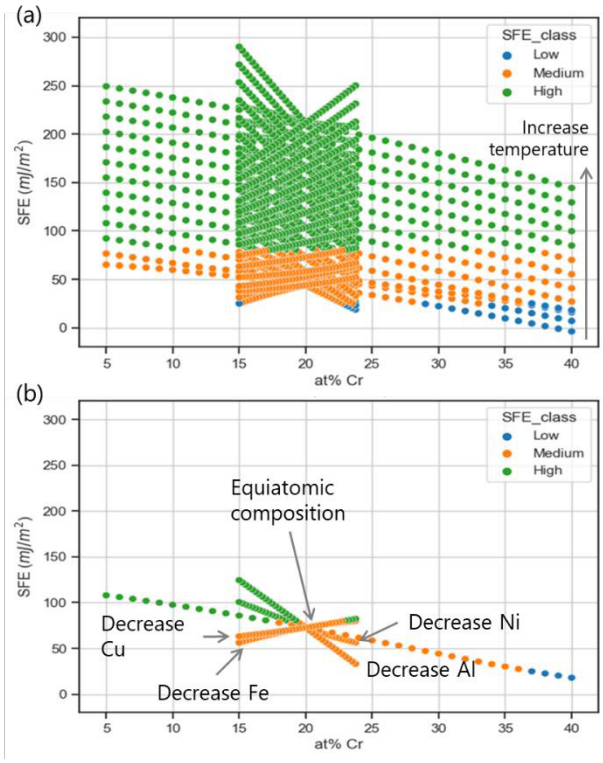

Fig. 6. Effect of Cr concentrations on the calculated SFE (a) at different temperatures from 1 to 1200 K and (b) at 300 K.

3.2.3 Effects of Al concentrations on SFE

Fig. 7 shows that with the increase of Al concentration, the SFE will increase significantly. For example, at a temperature of 300 K (Fig. 7(b)), the SFE increases from 33.1 mJ/m^2 to 124.42 mJ/m^2. Fig. 7(b) also shows the effect of other elements as the Al concentration increases, in which a decrease in Cr, Fe, and Cu increases the SFE, while a reduction of Ni can reduce the SFE. Kyung-Tae Park et al. shows that adding Al to Fe-22Mn-xAl-0.6C austenitic steel can increase the SFE[27]. They conclude that the increase in SFE due to the addition of Al can resist or delay the occurrence of mechanical twinning. In addition, research conducted by Sun et al. on HEA $Al_y(CrMnFeCoNi)_{1-y}$ alloy shows that the twinning ability will decrease due to the addition of Al atoms, and SFE will increase along with the concentration of Al[28]. This previous research supports our study that with the increase of Al concentrations, SFE will increase, and twinning will be more difficult.

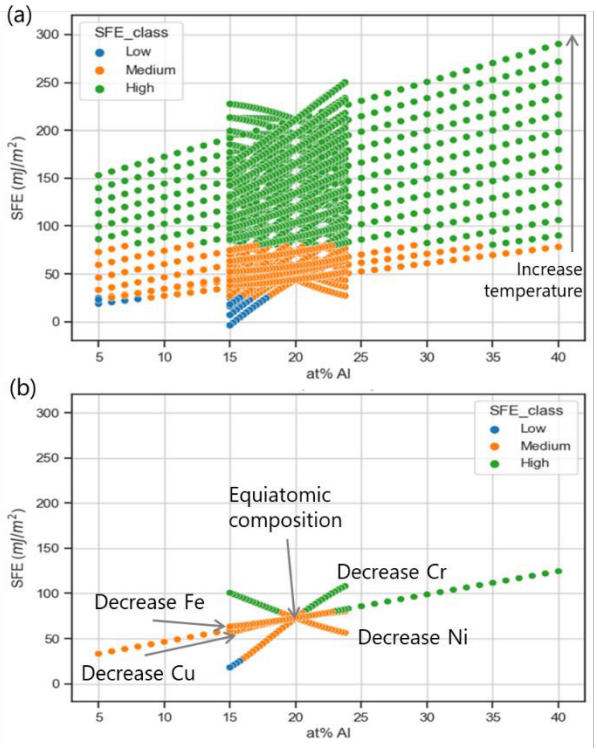

Fig. 7. Effect of Al concentrations on the calculated SFE (a) at different temperatures from 1 to 1200 K and (b) at 300 K.

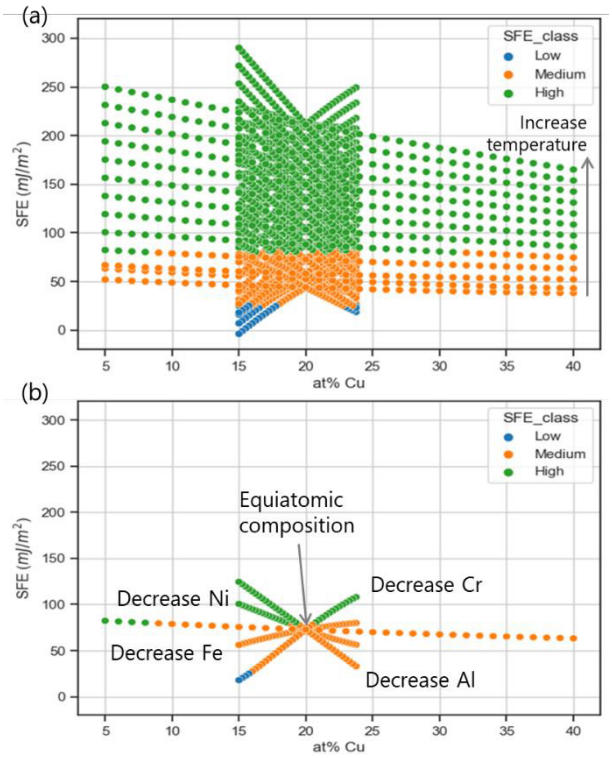

Fig. 8. Effect of Cu concentrations on the calculated SFE (a) at different temperatures from 1 to 1200 K and (b) at 300 K.

3.2.4 Effects of Cu concentrations on SFE

Similar to the effect of Cr, increasing Cu concentrations will decrease the SFE, as shown in Fig. 8. Compared to the effect of the other elements on the SFE, the reduction of SFE due to increased Cu concentrations is not significant. Fig. 8(b) shows that at a temperature of 300 K, the SFE decreased from 82.26 mJ/m^2 to 63.18 mJ/m^2. Fig. 8(b) also shows the effect of other elements as the Cu concentration increases, in which a decrease in Cr and Fe increases the SFE, while a reduction of Al and Ni can reduce the SFE. According to research by Lei Huang, adding Cu atoms as much as 0, 0.5, 1.0, 1.5, and 2.0 at.% in AlCrFeNiTiCu$_x$ alloy can increase the intensity of FCC phase[29]. This result means that as the Cu content in the alloy increases, the FCC stability will increase, and therefore the SFE increases. This result differs from the effect of Cu concentrations on the SFE in this study. This tendency can happen because, in the simulation from thermodynamic calculations, there is an influence from the concentrations of other more dominant elements. Given the insignificant effect of Cu addition, the effect of other elements can be dominant in the overall SFE calculation.

3.2.5 Effects of Fe concentrations on SFE

Similar to the effect of Cr and Cu, increasing Fe concentrations from 5 to 40 at.% shows a decrease in SFE at temperatures of 1 K to 900 K, as shown in Fig. 9. However, the SFE tends to increase with increasing Fe concentrations at a temperature above 900 K. For example, at 300 K, the SFE decreases from 79.93 mJ/m^2 to 56.14 mJ/m^2 (Fig. 9(b)), while at 1100 K, the SFE increases from 192.96 mJ/m^2 to 195.19 mJ/m^2. This can be explained according to thermodynamic calculations, where the value of $\Delta G_{Fe}^{\gamma\rightarrow\varepsilon}$ is a function of positive entropy, so as the temperature increases, the value will become positive at a certain point and change its contribution to the SFE to be positive. This shows that the effect of SFE can vary depending on the temperature and composition of Fe.

In general, the addition of Fe tends to decrease the SFE, because Fe has a relatively low SFE compared to other elements, and its presence in the crystal lattice can cause a reduction in the overall SFE. Research by Wang et al. gave similar results with Fe-Cr alloys, that the addition of Fe atoms can reduce the SFE[28]. The greater Fe concentrations in the alloy, the possibility of the alloy to undergo twinning deformation will increase as well.

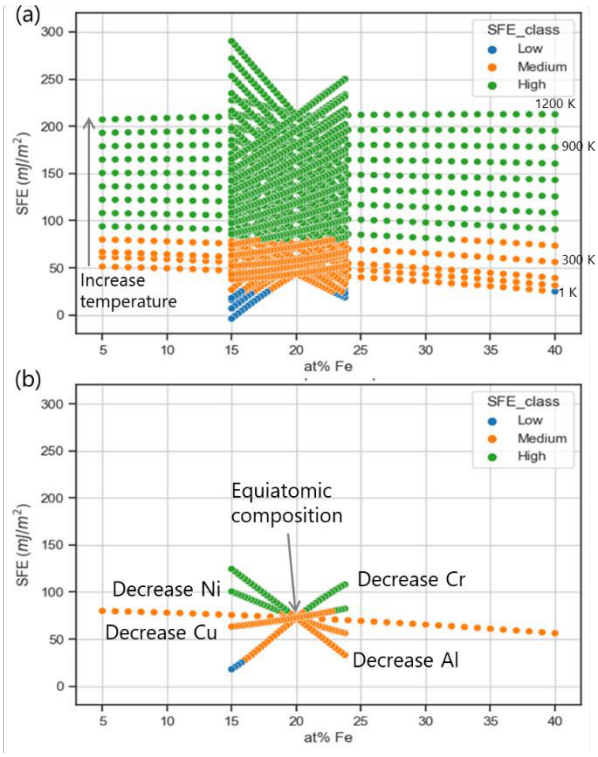

Fig. 9. Effect of Fe concentrations on the calculated SFE (a) at different temperatures from 1 to 1200 K and (b) at 300 K.

3.3 Machine Learning Model Evaluation

The machine learning model's performance was discussed and compared with the model prediction from thermodynamic calculation data and our previous result using the first-principle method[31]. The evaluation carried out uses root mean squared error (RMSE). Fig. 10 shows that the true values align with the prediction value, which means the model predicts the value accurately. The R-squared (R^2) for this model is 0.98, while the RMSE of this model is 0.005 for the training and 0.008 for the validation. This value means the model is not overfitting since the validation is not below the training RMSE and not underfitting since the training RMSE is already reaching a small error.

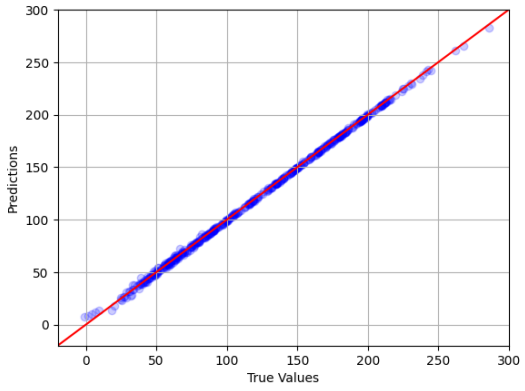

Fig. 10. True values vs. prediction values in a linear graph from deep neural network model.

Fig. 11 shows a visualization of how many of the predicted values in each SFE value are accurately predicted. The red bar indicates the actual value from the calculated SFE using a computational thermodynamic method, and the blue bar indicates the predicted values. It shows that the blue bar is covering up the red ones, which means it is accurately predicted. Nevertheless, an uncovered red bar indicates the error in the model.

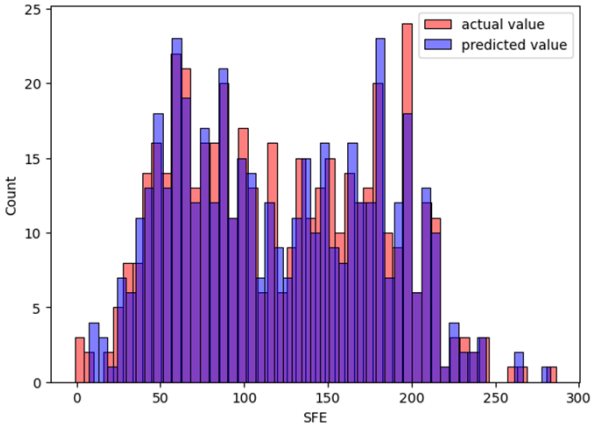

Fig. 11. Difference of actual value of SFE from the database and predicted value of SFE from deep neural network model.

The SFE of FeNiCrAl alloy was calculated based on thermodynamic and first-principle calculations in our previous work[31] and then compared with the prediction results of the machine learning model in this study. Table 1 shows that the SFE from the machine learning neural network model can predict the SFE close to the SFE of thermodynamic calculations but does not represent the results in the first-principle calculation. This tendency is because the training data used to train the model results from thermodynamic calculations, so the model is not trained with the results of the first-principle method. However, in equiatomic HEA $Fe_{25}Ni_{25}Cr_{25}Al_{25}$, the model can predict close to the first-principle value. This can happen because the value of thermodynamics is initially close to the value of the first-principles.

Table 1. Comparison of the calculated SFE and the classification from Computational Thermodynamic (CT), First-principle (FP), and Deep Neural Network (DNN) machine learning.

Temp. (K)	Alloy	SFE value (mJ/m²) and classification		
		CT	FP	DNN
0	$Fe_{25}Ni_{25}Cr_{25}Al_{25}$	55.22 (Med.)	52.22 (Med.)	52.89 (Med.)
0	$Fe_{25}Ni_{25}Cr_{30}Al_{20}$	40.86 (Med.)	24.51 (Low)	39.16 (Med.)
0	$Fe_{25}Ni_{30}Cr_{25}Al_{20}$	56.82 (Med.)	72.2 (Med.)	55.48 (Med.)

Note: CT: Computational Thermodynamic, FP: First-principle, DNN: Deep Neural Network, Med.: Medium

Therefore, the main difference that occurs here is the difference between the thermodynamic calculation method and the first-principle method, which can happen for several reasons, including 1) different method approaches, in the first-principle, SFE is

measured with a quantum mechanical theory approach such as its atomic structure. While in thermodynamic calculations, the approach is done through Gibbs energy by Olson and Cohen[17], which is very dependent on temperature and alloy composition, and 2) temperature are not precisely the same because the thermodynamic database is not used for calculation below room temperature (298 K), so they are approached to 1 K, while in the first-principle calculations still in absolute zero temperature (0 K).

3.4 Designing Fe-based High Entropy Superalloy FeNiCrAlCu for High Temperature Applications

Designing a high entropy superalloy (HESA) requires considering various factors, including elemental determination, atomic percentages, and desired alloy properties. The desired alloy properties in high-temperature applications are strength, toughness, oxidation resistance, and good thermal stability. HESA are new alloys developed to provide alternative alloys at high temperatures with properties that are not inferior to superalloys. Yeh et al. study the HESA AlCoCrFeNiTi alloy that offers excellent properties such as high γ' solvus temperature and a stable γ-γ' microstructure without any detrimental phase formation[32]. The high-temperature strength of HESA is attributed to the high-volume fraction of γ' precipitates, high degree of solid solution strengthening due to the distortion lattice, and the increase in anti-phase boundary (APB) energy, which results in more energy for dislocation pairs to intersect the γ'.

HESA also has a light density (below 8 g/cm^3) with raw material costs 20% lower than first-generation super alloys such as CM247LC. This can be achieved because the use of Fe and Ti is increased, while high-value elements such as Ni and refractory elements are minimized. HESA in the study by Yeh showed the bcc phase formation at low temperatures. However, isothermal aging at 700^{o}C showed thermal stability of γ' precipitates due to the nature of the HEA, which tends to have a sluggish phase transformation rate[32]. Lattice misfit (δ) is one of the main factors in directional coarsening of γ' known as "rafting". With a negative value of lattice misfit, it can effectively restrain dislocation climb and produce creep resistance[33]. The role of HESA can be attributed to expanding the lattice misfit in the negative direction, which can be achieved by forming γ and γ' phases not limited to Al, Co, Cr, Fe, Ni, and Ti. In addition, the high activity of Cr and Al implies continuous Cr_2O_3 and Al_2O_3 that can form rapidly when exposed to oxidative environments at high temperatures.

In HESA FeNiCrAlCu, Ni is the main contributor to the thermal stability of matrix γ and precipitates γ', with the addition of Fe, Cr, and Cu, which can reduce the SFE, a lower SFE in HESA can be expected. This can be confirmed through the research conducted by Te-Kang Tsao et al., who explained with the optimization parameter of SFE described as $\delta\Gamma_i$, by applying a certain composition to the model $\Delta_\Gamma^\gamma(x) = \sum_i x_i \delta\Gamma_i$[34]. this equation showed an indication of a decrease in SFE ($\Delta_\Gamma^\gamma(x)$) in the fcc matrix due to the element concentrations that decrease SFE into HESA (x). In addition, elements that contribute to forming γ' can significantly increase the APB energy, which can strengthen HESA[35]. The correlation between SFE, creep activation energy, and creep strain rate can be described as the following equation[36]:

$$\dot{\epsilon} = A' \left(\frac{\gamma_{sf}}{Gb}\right)^3 (\sigma G)^5 \exp\left(-Q/RT\right) \quad (1)$$

where A' is a constant, γ_{sf} is stacking fault energy, G is shear modulus, b is Burger's vector, Q is activation creep energy, and σ is applied stress, so decreasing SFE and increasing Q of HESA can reduce the creep rate[36]. In materials with low SFE, partial dislocations are energetically easier to occur, and the distance between partial dislocations can be increased, resulting in dislocation bowing around the γ' particle becoming more complicated and effectively reducing the creep rate.

Based on the provisions discussed, the optimal composition of the HESA FeNiCrAlCu is sought to meet the prerequisites of HESA and adjust the composition that tends to decrease the SFE to initiate deformation twinning and reduce the creep rate. The classification of the SFE used in this study is the classification conducted by Hamada and Vecammen, which ranges from low (below 25 mJ/m^2), medium (25 mJ/m^2 to 80 mJ/m^2), and high (above 80 mJ/m^2)[37]. It is important to note that the classification of SFE itself is not absolute, as the alloy composition and processing methods can significantly affect the mechanical properties. Therefore, it is crucial to evaluate each alloy's mechanical properties and potential applications[38].

Table 2 presents the optimum composition that tends to produce low and medium SFE classification. Based on Fig. 4 until Fig. 8, Al and Cr significantly affect the SFE, which means it can become the determinant for the design of HESA FeNiCrAlCu. Fe and Ni is also crucial because it is the main component which stabilize the preferred microstructure γ and γ' phases.

Table 2. Optimum composition for designing HESA FeNiCrAlCu based on the SFE calculations in this study.

Element	Atomic percent (at. %)
Ni	9-15
Cr	15-36
Al	5-22.75
Cu	9-22.75
Fe	22.75-40

Fig. 12 can be used as a guideline for a composition of HESA FeNiCrAlCu to achieve a low SFE and twinning deformation. For example, high entropy alloy with a composition of Al-5% and Cr-25% $Fe_{23.3}Ni_{23.3}Cr_{25}Al_5Cu_{23.3}$ will have the SFE of 50.25 mJ/m^2 (Fig. 12(a)) and the Fe-based HESA with a

composition of Fe-35% and Ni-25% $Fe_{35}Ni_{25}Cr_{13.3}Al_{13.3}Cu_{13.3}$ will have the SFE of 60.40 mJ/m^2 (Fig. 12(b)). Both alloys produce relatively low SFE and are classified as medium SFE, which is expected to have a dominant deformation mechanism of twinning. With deformation twinning, the alloy will have good toughness and an equilibrium between the ductility and brittleness of the material. Then, it has optimal strength and the tendency of low SFE, which can improve creep resistance.

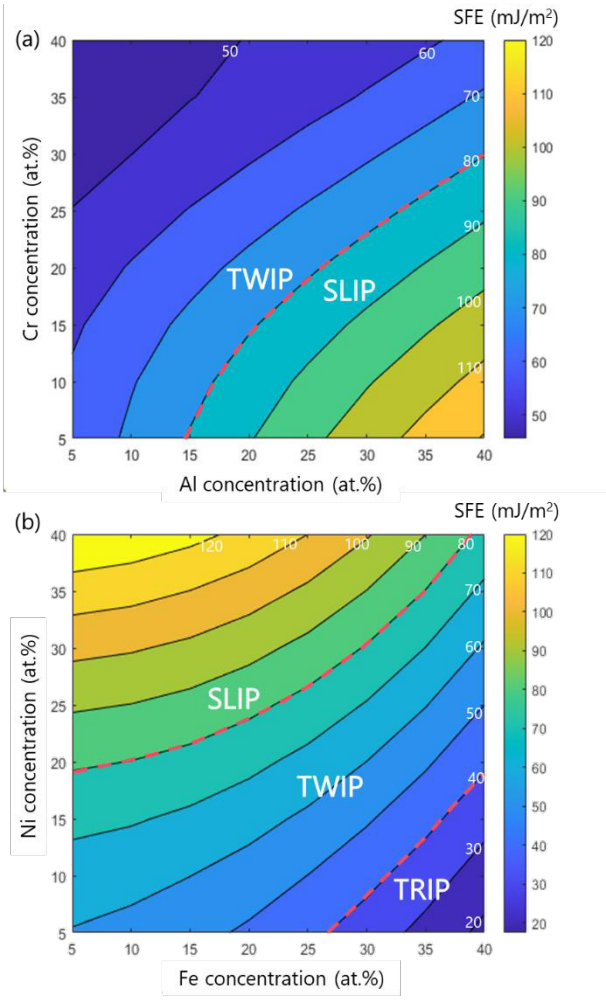

Fig. 12. Deformation map and the calculated SFE as a function of (a) Al and Cr concentrations, (b) Fe and Ni concentrations for designing HESA FeNiCrAlCu with deformation mechanism of TWIP (Twinning Induced Plasticity).

4 Conclusions

1. The SFE of non-equiatomic Fe-based HESA FeNiCrAlCu can be lower than equiatomic HEA FeNiCrAlCu. However, it also depends on the composition of the elements. Increasing concentrations of Ni and Al increases the SFE, while increasing concentrations of Fe, Cr, and Cu decreases the SFE. An increase in mixing entropy can generally reduce the SFE.

2. Magnetic contributions play a significant role at low temperatures and decrease with increasing temperature, and then the SFE increases with temperature. Some compositions of Fe-based HESA can have a lower SFE at low temperatures, but they can change at high temperatures.

3. The machine learning model built with deep learning neural network architecture achieved the Root Mean Squared Error of 0.005 for the training and 0.008 for validation, which means the model can accurately predict the SFE of FeNiCrAlCu alloy with different compositions and temperatures. The importance factor of Fe and Ni concentrations lower than Al and Cr concentrations means that Ni can be replaced by Fe or concentrations of Fe can be increased as an alloy base without significantly changing the SFE or, even better, lowering the SFE.

4. The optimum compositions of HESA FeNiCrAlCu are produced with a lower SFE than equiatomic HEA FeNiCrAlCu, even at high temperatures. Fe can be increased until 40 at.% with 15 at.% Ni, or Ni can be reduced until 9 at.% with a lower Fe of 22.75 at.%. FeNiCrAlCu high entropy superalloy design aims to obtain SFE in the 25-80 mJ/m^2 range to obtain dominant twinning deformation so that cross slip decreases and creep resistance increases.

Acknowledgments

This work was supported by the Research, Community Service, and Innovation (PPMI) Program ITB 2023, the Research Program ITB 2021 (FTTM.PN-6-17-2021) and Research and Innovation Program for Advanced Indonesia (RIIM) 2022 BRIN.

References

1. A.P. Mouritz, *Superalloys for gas turbine engines Introduction to Aerospace Materials*, Woodhead Publishing: Cambridge, (2012)
2. C. T. Sims, N. S. Stoloff, and W. C. Hagel, *superalloys* II vol. 8, Wiley New York, (1987).
3. R.C. Reed, Roger C., *The superalloys : fundamentals and applications*, Cambridge University Press, (2006)
4. S. Chen, Q. Li, J. Zhong, F. Xing, and L. Zhang, *On diffusion behaviors in face centered cubic phase of Al-Co-Cr-Fe-Ni-Ti high-entropy superalloys*, J Alloys Compd, **791**, 255–264, (2019)
5. Y.-T. Chen, Y.-J. Chang, H. Murakami, S. Gorsse, A.-C. Yeh, *Designing high entropy superalloys for elevated temperature application*, Scr Mater, **187**, 177–182, (2020).
6. E. P. George, D. Raabe, R. O. Ritchie, *High-entropy alloys*, Nat Rev Mater, **4**, no. 8, 515–534, (2019)
7. D. Miracle, J. Miller, O. Senkov, C. Woodward, M. Uchic, J. Tiley, *Exploration and Development of High Entropy Alloys for Structural Applications*, Entropy, vol. **16**, no. 1, pp. 494–525, (2014)

8. J.-W. Yeh et al., *Nanostructured High-Entropy Alloys with Multiple Principal Elements: Novel Alloy Design Concepts and Outcomes*, Adv Eng Mater, vol. **6**, no. 5, pp. 299–303, (2004)
9. D. B. Miracle, O. N. Senkov, *A critical review of high entropy alloys and related concepts*, Acta Mater, vol. **122**, pp. 448–511, (2017)
10. Y. Yin et al., *High-temperature age-hardening of a novel cost-effective Fe45Ni25Cr25Mo5 high entropy alloy*, Materials Science and Engineering: A, vol. **788**, p. 139580, (2020)
11. S. Li et al., *Cost-efficient copper-nickel alloy for active cooling applications*, Int J Heat Mass Transf, vol. **195**, p. 123181, (2022)
12. W. D. Wong-Ángel, L. Téllez-Jurado, J. F. Chávez-Alcalá, E. Chavira-Martínez, V. F. Verduzco-Cedeño, *Effect of copper on the mechanical properties of alloys formed by powder metallurgy*, Mater Des, vol. **58**, pp. 12–18, (2014)
13. L. Huang, *Effect of Cu segregation on the phase transformation and properties of AlCrFeNiTiCux high-entropy alloys*, Intermetallics **140**, 107397 (2022)
14. B. Li, E. J. Lavernia, Y. Lin, F. Chen, L. Zhang, *Spray Forming of MMCs in Reference Module in Materials Science and Materials Engineering*, Elsevier, (2016)
15. ASM International, *ASM Handbook Volume 2: Properties and Selection: Nonferrous Alloys and Special-Purpose Materials*, vol. 2. (2002)
16. P. J. Ferreira, P. Müllner, *A thermodynamic model for the stacking-fault energy*, Acta Mater, vol. **46**, no. 13, pp. 4479–4484, (1998)
17. T. L. Achmad, W. Fu, H. Chen, C. Zhang, Z.-G. Yang, *Effects of alloying elements concentrations and temperatures on the stacking fault energies of Co-based alloys by computational thermodynamic approach and first-principles calculations*, J Alloys Compd, vol. **694**, pp. 1265–1279, (2017)
18. A. Van De Walle M. Asta, *High-throughput calculations in the context of alloy design*, MRS Bull, vol. **44**, no. 4, pp. 252–256, (2019)
19. T. Borkar, *A combinatorial assessment of $AlxCrCuFeNi_2$ complex concentrated alloys: Microstructure, microhardness, and magnetic properties*, Acta Mater **116**, 63–76 (2016)
20. H. Gholizadeh, *The Influence of Alloying and Temperature on the Stacking-fault Energy of Iron-based Alloys*, Montanuniversität Leoben, (2013)
21. Y. H. Zhang, Y. Zhuang, A. Hu, J.-J. Kai, and C. T. Liu, "The origin of negative stacking fault energies and nano-twin formation in face-centered cubic high entropy alloys," Scr Mater, vol. **130**, pp. 96–99, (2017).
22. F. Zhang et al., *Polymorphism in a high-entropy alloy*, Nat Commun, vol. **8**, no. 1, p. 15687, (2017)
23. Z. Y. Wang, D. Han, X. W. Li, *Competitive effect of stacking fault energy and short-range clustering on the plastic deformation behavior of Cu-Ni alloys*, Materials Science and Engineering: A, vol. **679**, pp. 484–492, (2017)
24. J.-Q. Zhao, H. Tian, Z. Wang, X.-J. Wang, J.-W. Qiao, *FCC-to-HCP Phase Transformation in CoCrNix Medium-Entropy Alloys*, Acta Metallurgica Sinica (English Letters), vol. **33**, no. 8, pp. 1151–1158, (2020)
25. A. Dumay, J.-P. Chateau, S. Allain, S. Migot, O. Bouaziz, *Influence of addition elements on the stacking-fault energy and mechanical properties of an austenitic Fe–Mn–C steel*, Materials Science and Engineering: A, vol. 483–484, pp. 184–187, (2008)
26. J. Yan et al., *Plastic deformation mechanism of CoCrxNi medium entropy alloys*, Materials Science and Engineering: A, vol. **814**, p. 141181, (2021)
27. K.-T. Park, K. G. Jin, S. H. Han, S. W. Hwang, K. Choi, C. S. Lee, *Stacking fault energy and plastic deformation of fully austenitic high manganese steels: Effect of Al addition*, Materials Science and Engineering: A, vol. **527**, no. 16–17, pp. 3651–3661, (2010)
28. X. Sun, H. Zhang, W. Li, X. Ding, Y. Wang, L. Vitos, *Generalized Stacking Fault Energy of Al-Doped CrMnFeCoNi High-Entropy Alloy*, Nanomaterials, vol. **10**, no. 1, p. 59, (2019)
29. L. Huang, X. Wang, B. Huang, X. Zhao, H. Chen, C. Wang, *Effect of Cu segregation on the phase transformation and properties of AlCrFeNiTiCux high-entropy alloys*, Intermetallics (Barking), vol. **140**, p. 107397, (2022)
30. C. Wang, S. Schönecker, W. Li, Y. Yang, Q.-M. Hu, L. Vitos, *Twinning pathways in Fe and Fe–Cr alloys from first-principles theory*, Acta Mater, vol. **215**, p. 117094, (2021).
31. A. Zamani, *Pemodelan Stacking Fault Energy Dengan Metode Komputasi Untuk Desain Paduan Entropi Sedang CoCrNiAl dan FeCrNiAl pada Aplikasi Biomedis*, (2021).
32. A. C. Yeh et al., *Developing new type of high temperature alloys–high entropy superalloys*, Int. J. Metall. Mater. Eng, vol. **1**, no. 107, pp. 1–4, (2015)
33. J. X. Zhang, J. C. Wang, H. Harada, Y. Koizumi, *The effect of lattice misfit on the dislocation motion in superalloys during high-temperature low-stress creep*, Acta Mater, vol. **53**, no. 17, pp. 4623–4633, (2005)
34. T.-K. Tsao et al., *The high temperature tensile and creep behaviors of high entropy superalloy*," Sci Rep, vol. 7, no. **1**, p. 12658, (2017)
35. T.-K. Tsao, A.-C. Yeh, *The thermal stability and strength of highly alloyed Ni_3Al*, Mater Trans, vol. **56**, no. 11, pp. 1905–1910, (2015)
36. F. R. N. Nabarro, F. L. de Villiers, *Physics of creep and creep-resistant alloys*, CRC press, (1995)
37. N. Chaudhary, A. Abu-Odeh, I. Karaman, R. Arróyave, *A data-driven machine learning approach to predicting stacking faulting energy in*

austenitic steels, J Mater Sci, vol. **52**, pp. 11048–11076, (2017)

38. T.L Achmad, *Development of Stacking Fault Energy (SFE) Modelling of Co-based Alloys for Alloy Design*, Tsinghua University, (2018)